Nuclear Physics **A473** (1987) 160–178
North-Holland, Amsterdam

ELECTROEXCITATION OF ^{58}Ni: A study of the fragmentation of the magnetic dipole strength*

W. METTNER[1], A. RICHTER and W. STOCK[2]

Institut für Kernphysik der Technischen Hochschule Darmstadt, D-6100 Darmstadt, F.R. Germany

B.C. METSCH

Institut für Theoretische Kernphysik der Universität Bonn, D-5300 Bonn, F.R. Germany

A.G.M. VAN HEES

Fysisch Laboratorium der Rijksuniversiteit Utrecht, Utrecht, The Netherlands

Received 11 June 1987

Abstract: The distribution of the magnetic dipole strength in ^{58}Ni in the excitation energy range $E_x = 6$–15 MeV has been studied with high resolution inelastic electron scattering. Altogether 47 $J^\pi = 1^+$ states have been determined. The summed M1 strength is $\sum B(\mathrm{M1})\uparrow = 16.9^{+4.6}_{-3.3}\mu_N^2$. A shell model calculation including 1p-1h excitations is used to discuss the fragmentation, the summed strength and the relative importance of spin versus orbital magnetism. By comparison with inelastic proton scattering and charge exchange reactions the isospin structure of the M1 strength distribution is analysed.

E | NUCLEAR REACTION ^{58}Ni(e, e'), $E = 39$–57 MeV; measured $\sigma(E(e'))$, $\sigma(\theta)$. ^{58}Ni deduced $B(\lambda)$. Comparison with shell model calculation.

1. Introduction

In recent years the magnetic dipole strength distribution in the fp-shell nuclei ^{40,42,44,48}Ca and in the $N = 28$ isotones ^{50}Ti, ^{51}V, ^{52}Cr and ^{54}Fe has been studied with high resolution inelastic electron scattering with the DALINAC [1–7]). To complete the analysis of the $1f_{7/2} \rightarrow 1f_{5/2}$ spin-flip M1 excitations the most natural choice would be the double magic nucleus $^{56}_{28}Ni_{28}$ which, however, is unstable. Therefore as a substitute we investigated ^{58}Ni.

The electron scattering data on ^{58}Ni available up to now enabled the determination of some M1 transitions but their insufficient energy resolution hampered a reliable estimate of the transition strength [8]). This is demonstrated in fig. 1. A precise transition strength is necessary, however, to draw conclusion to the following issues: (i) For medium heavy nuclei a quenching of the M1 strength has been observed [9]).

* Work supported by Deutsche Forschungsgemeinschaft.

[1] Present address: Aristo GmbH., Hamburg, Germany.

[2] Present address: Schenk AG, Darmstadt, Germany.

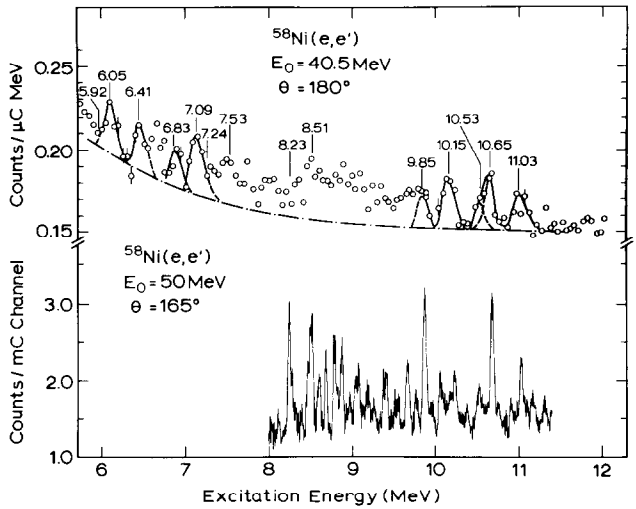

Fig. 1. Comparison of a 180° inelastic electron scattering spectrum on ^{58}Ni taken with medium energy resolution at the old Naval Research Laboratory accelerator [8]) and a 165° spectrum from the Darmstadt electron accelerator DALINAC.

How does ^{58}Ni fit into the systematics found? (ii) The nucleus ^{58}Ni has isospin $T_0 = 1$ in its ground state which implies $T_0 \rightarrow T_0$ and $T_0 \rightarrow T_0 + 1$ M1 transitions. How large is the isospin splitting between the J^π; $T = 1^+$; 1 and 1^+; 2 states, respectively? (iii) Similar as in the case of the $N = 28$ isotones, in ^{58}Ni neutrons *and* protons participate in the M1 transition. This immediately implies the existence of spin and orbital magnetism, which could be clarified by a comparison of the present (e, e') data with high resolution inelastic protons scattering data [10]) and reliable shell model calculations [11]). (iv) Finally, an absolute determination of the M1 transition strength can be used to calibrate the strength of Gamow-Teller processes such as inverse β-decay which is an important ingredient in supernova dynamics [12–19]).

The experimental technique, the electron scattering spectra and the extraction of the transition strength are described in sect. 2. A discussion of the results including a comparison with shell model calculations and the results from other spin flip probing reactions is made in sect. 3. and conclusions are drawn in sect. 4.

2. Experimental technique, spectra and transition strength

2.1. TECHNIQUE

The experiment has been performed with the energy-loss electron scattering facility and the Darmstadt electron linear accelerator (DALINAC) documented elsewhere [20]). The stability of the system which is now in continuous operation since 1975 is illustrated in fig. 2. Two spectra taken at the same incident electron energy $E_0 = 50$ MeV and scattering angle $\Theta = 165°$ but about half a year apart in time are

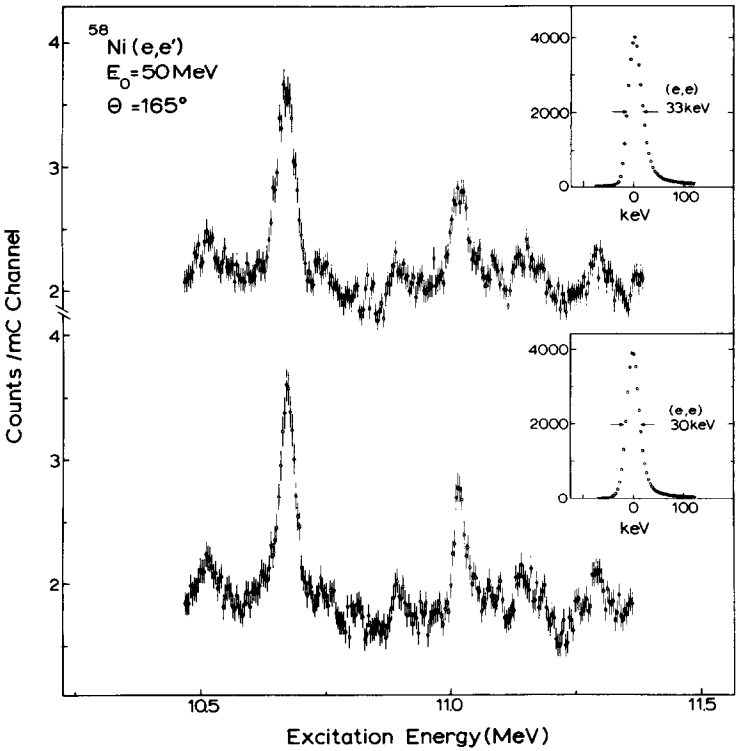

Fig. 2. Two ^{58}Ni(e, e') spectra accumulated at the same energy $E_0 = 50$ MeV and scattering angle $\Theta = 165°$, but about 6 months apart in time. The respective energy resolution of each spectrum is indicated through the width of the elastic lines which are plotted as inserts. Almost every detail in the two spectra is identical indicating the high reproducibility obtainable for (e, e') spectra at the DALINAC.

compared with each other. The respective energy resolutions of $\Delta E_{1/2} = 33$ and 30 keV (FWHM) can be inferred from the width of the elastic lines shown as an insert in the figure. Almost every detail is reproduced in the two spectra which were accumulated in a region of high excitation and high level density in ^{58}Ni.

The ^{58}Ni target (enriched to 99.89%) consisted of a 13.5 μm thick foil ($\rho x = 12$ mg/cm^2). With this target fifteen spectra were accumulated for bombarding energies $E_0 = 39.4$ to 57.3 MeV and magnetic spectrometer angle settings $\Theta = 93°$ to 165°. Depending upon the reflection or transmission geometry of the target and on the bombarding energy the energy resolution in the spectra varied between $\Delta E_{1/2} = 24$ to 47 keV. Each spectrum took between 50 to 140 h of run time so that the whole experiment consumed well over 1000 h.

2.2. SPECTRA

A spectrum surveying the excitation energy range from $E_x = 2.5$ to 15 MeV is shown in fig. 3. In order to exhibit for this spectrum the predominantly longitudinal

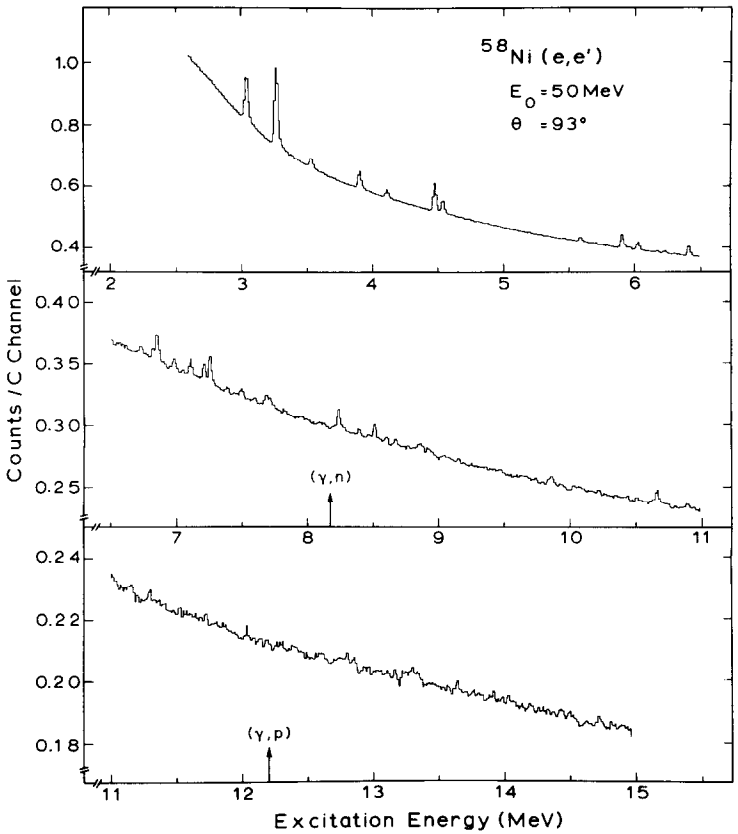

Fig. 3. Survey ^{58}Ni(e, e') spectrum at $E_0 = 50$ MeV and $\theta = 93°$ covering an excitation energy range from $E_x = 2.5$ to 15 MeV. The proton- and neutron thresholds at 8.2 and 12.2 MeV, respectively, are indicated by arrows.

electric excitations at low excitation energies, an incident electron energy of $E_0 =$ 50 MeV and a scattering angle of $\Theta = 93°$ has been chosen. The spectrum reveals three distinctly different regimes of excitation. Relatively strong transitions give rise to lines on a smooth background mainly due to the radiative tail of the elastic line (upper part of fig. 3). Fairly intense lines are still visible up to energies around the threshold for proton emission, but the background in the spectrum becomes already structured indicating the existence of closely lying and partly overlapping lines (middle part). Finally, with increasing excitation energy (lower part) the number of lines in the spectrum increases also and the experimental energy resolution $\Delta E = 24$ keV (FWHM) is not sufficient anymore to resolve all details of the spectrum.

Since the main interest of the present work was focussed onto M1 excitations at excitation energies $E_x > 6$ MeV further spectra were only measured at higher energies. In fig. 4 three spectra recorded at a constant momentum transfer $q = 0.37$ fm^{-1} for $E_x = 5.7$–8.0 MeV are shown. Some of the J^π; $T_0 = 1^+$; 1 states were expected in this

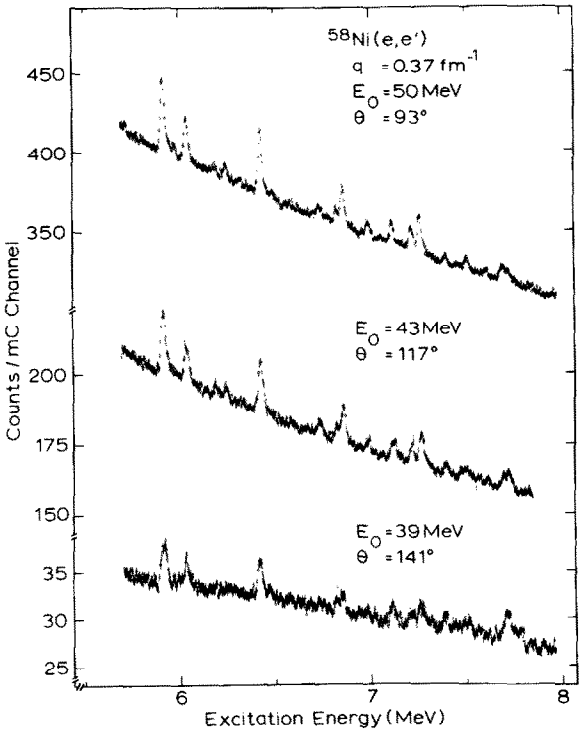

Fig. 4. Three ^{58}Ni(e, e') spectra taken at constant momentum transfer $q = 0.37$ fm^{-1}. The various combinations of incident electron energies and scattering angles are indicated on the figure.

excitation energy range but the behaviour of the decreasing transition strength from the forward angle to the backward angle spectra indicate the longitudinal nature of the excitation of most of the peaks.

Figure 5 summarizes four ^{58}Ni(e, e') spectra all measured at an incident electron energy $E_0 = 50$ MeV. An excitation energy range $E_x = 9.3$–11.1 MeV has been covered in which predominantly J^π; $T_0+1 = 1^+$; 2 states should have been excited, and indeed the increase in the transition strength of most peaks at backward angles is characteristic for the existence of predominantly transverse excitations. Note, however, that the achieved energy resolution in those spectra (measured at the fairly isolated level at $E_x = 10.670$ MeV) is not anymore sufficient to resolve peaks corresponding to single levels.

Finally, fig. 6 shows three spectra at various incident energy and scattering angle combinations resulting in a constant momentum transfer $q = 0.49$ fm^{-1}. Because of the very large number of data points in each spectrum a histogram plot has been chosen. Up to $E_x \approx 11$ MeV one notices the same transverse behaviour of the transition strength as is evident from fig. 5. Above this energy strong transitions cease to exist and the analysis of the spectra to be discussed next has yielded about

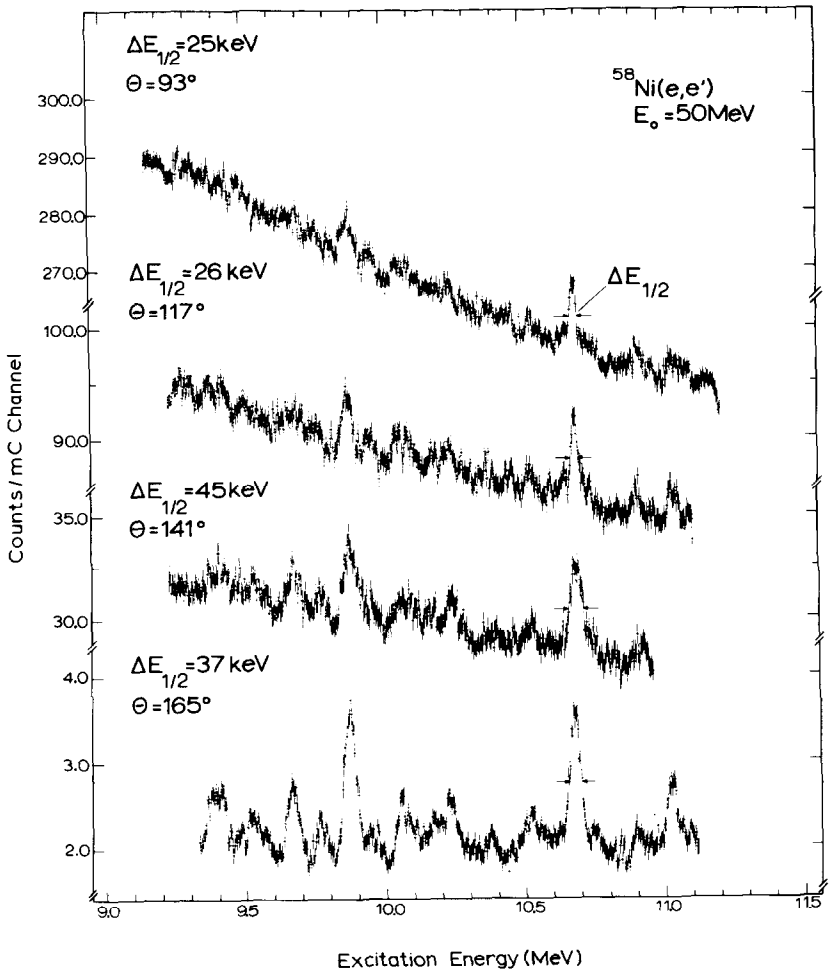

Fig. 5. Four ^{58}Ni(e, e') spectra measured at $E_0 = 50$ MeV but various scattering angles. The energy resolution $\Delta E_{1/2}$(FWHM) of each spectrum determined from the width of the fairly isolated peak at $E_x = 10.670$ MeV is indicated on the figure.

an equal number of longitudinal and transverse transitions responsible responsible for the observed strength in the spectra.

2.3. ANALYSIS OF SPECTRA, EXCITATION ENERGIES AND TRANSITION STRENGTHS

The analysis of the measured spectra with the objective to obtained reliable excitation energies and transition strengths has been performed entirely consistent with the one employed in previous high resolution inelastic electron scattering experiments at the DALINAC. Since this analysis has been documented already several times (see e.g. refs. [4,6,7,21]) one can be brief here.

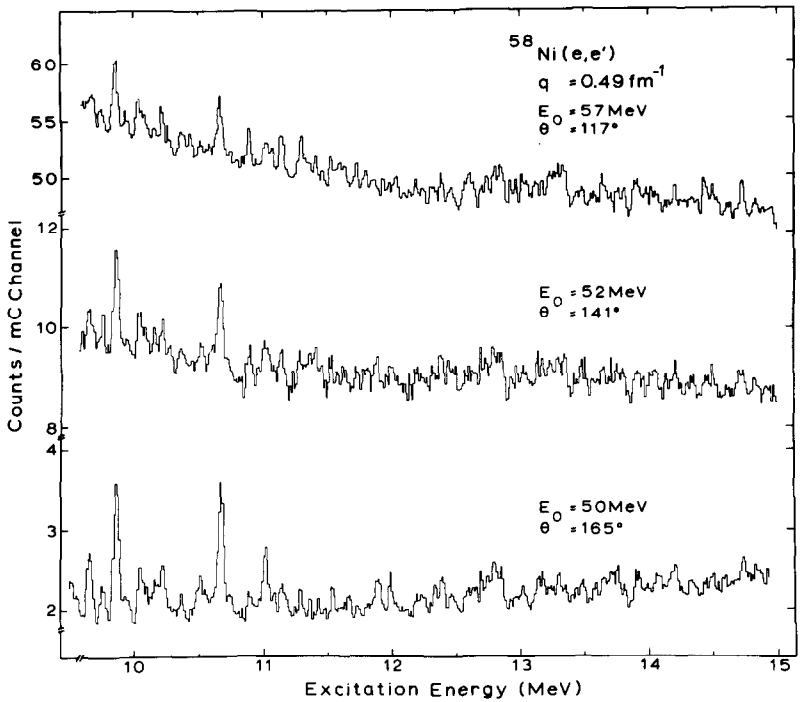

Fig. 6. Three ^{58}Ni(e, e') spectra covering the excitation energy range from $E_x \approx 10$–15 MeV. These spectra were taken at the same momentum transfer $q = 0.49$ fm^{-1}.

Firstly, the background mainly due to the radiative tail of the elastic line has been subtracted by fitting a polynomial to each spectrum. Secondly, the spectra were then decomposed into individual lines by taking the line shape of the elastic line as a parameter. This resulted in a consistent set of excitation energies for [162] levels in ^{58}Ni between $E_x = 5.9$–14.9 MeV. Thirdly, the differential cross section for the excitation of each of these levels has been determined by comparing the area under the peaks to the area of the peak of the elastically scattered electrons and this ratio has been properly corrected for Schwinger-, bremsstrahlungs- and dispersion effects. The cross section for elastic scattering was computed in distorted wave Born approximation (DWBA). Input parameters into the phase shift program were the half density radius $c = 4.140$ fm and the skin thickness $t = 2.461$ fm of a two-parameter Fermi distribution approximating the ground state charge density distribution [22]).

Finally, the measured cross sections have been compared to theoretically calculated cross sections in DWBA in order to derive the multipolarity and strength of each transition. Since the momentum transfer in the present experiment is way below 1 fm^{-1}, DWBA cross sections were only computed for transitions with a multipolarity up to $\lambda = 4$. The necessary transition densities have been determined

in a shell model calculation with the modified surface delta interaction (MSDI) as residual interaction [11]). The model space was composed of 18 active nucleons outside a ^{40}Ca core. Between 15 and 16 nucleons occupied the $1f_{7/2}$ shell and the remaining 2 to 3 nucleons were distributed amongst the $2p_{3/2}$, $1f_{5/2}$ and $2p_{1/2}$ shells. Excitations into the $1g_{9/2}$ shell were also allowed. The model space for the particle-hole transitions in ^{58}Ni has thus for the transitions from the ground state into states of positive parity the structure $1f_{7/2}^{-1}(r)^3 \rightarrow (r)^2$ and into states of negative parity the structure $1f_{7/2}^{-1}(r)^2 1g_{9/2} \rightarrow (r)1g_{9/2}$ with the valence shells denoted by $r = (2p_{3/2}, 1f_{5/2}, 2p_{1/2})$. The respective transition densities have been inserted into a DWBA program [23]) and theoretical form factors F_λ of multipolarity λ were calculated, altogether 56 from the shell model calculations. Different from factors for a given multipolarity λ often exhibited a similar shape - they scaled - and the variance in this scaling, which has been discussed in detail in [21]), reflects itself in the uncertainty of the respective transition strength listed below.

All theoretical form factors have been compared with all measured form factors in a one parameter, error weighted fit, the one parameter being essentially the transition strength [21]). A definite multipolarity has only been assigned to a particular transition when all theoretical form factors for a given multipolarity have resulted in a satisfactory fit, otherwise the assignment has been ambiguous. Some examples of this comparison between experiment and theory for representative E1, E2, E3 and M1, M2 transitions are shown in fig. 7. Note that the measurements were not only performed at different incident energies but also at four different scattering angles and that one of the important criteria for a proper assignment of multipolarity and strength to a particular transition has been the requirement that the sometimes very different cross sections under different scattering angles - as can be seen in fig. 7 for the purely transverse M1 and M2 transitions - were well described.

In addition to the DWBA analysis of the experimental cross sections an analysis in terms of the plane wave Born approximation (PWBA) has also been attempted as for other fp-shell nuclei [5,7]). Despite the fact that the condition for the true applicability of such a procedure (i.e. $\alpha Z \ll 1$ with α being the fine structure constant and Z the number of target protons with $\alpha Z \approx 0.2$, is not fulfilled, results in very good agreement with the ones from the DWBA analysis have been obtained, in particular for the strong transitions, after proper DWBA corrections [24]) have been applied to the PWBA results. The PWBA method has of course the immediate advantage over the DWBA method that a separation of longitudinal and transverse parts of the measured cross section in terms of a Rosenbluth plot might be performed. The PWBA and DWBA results for the five strongest M1 transitions into the $T_0 + 1 = 2$ states are compared with each other in table 1. There is in all cases agreement between the transition strengths within the given uncertainties.

Table 2 summarizes the determined excitation energies E_x and the assigned J^π values for all 162 observed levels in ^{58}Ni between $E_x \approx 5.9$–15.0 MeV. The uncertainty in E_x is about $\pm$(5–8) keV in the region from 6–9 MeV and $\pm$(8–10) keV at higher

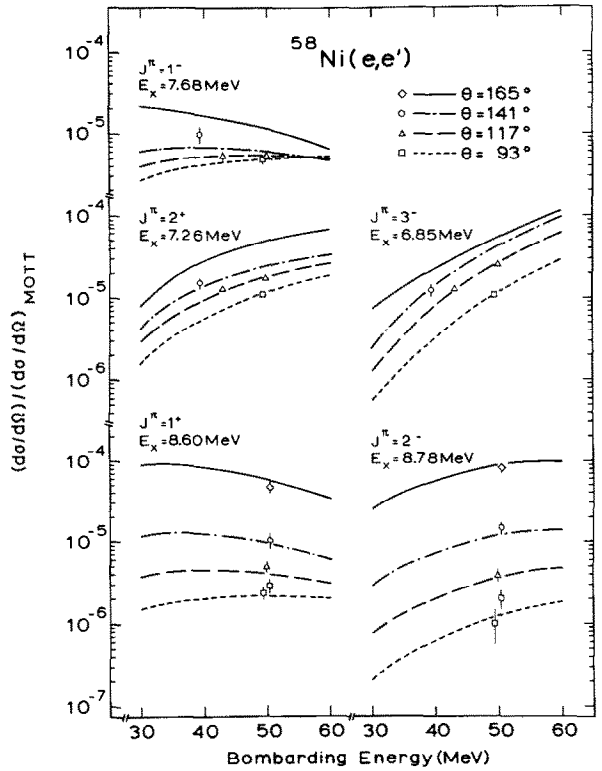

Fig. 7. Comparison of theoretical form factors for states with $J^\pi = 1^-$, 2^+, 3^-, 1^+ and 2^- in ^{58}Ni with experimental form factor points measured at various incident electron energies and at the scattering angles marked by different symbols in the insert of the figure.

TABLE 1

Comparison of the reduced M1 transition strengths of five transitions into J^π, $T_0+1=1^+$; 2 states in ^{58}Ni from a PWBA and a DWBA analysis. The derived transition radii from the PWBA analysis are also given

E_x [MeV]	$B(M1)\uparrow_{PWBA}$ [μ_N^2]	R_{tr} [fm]	$B(M1)\uparrow_{DWBA}$ [μ_N^2]
9.846	0.60 ± 0.14	3.7 ± 0.3	0.54 ± 0.16
10.218	0.40 ± 0.18	4.3 ± 0.5	0.56 ± 0.14
10.514	0.46 ± 0.15	3.8 ± 0.4	0.40 ± 0.10
10.670	1.56 ± 0.16	4.0 ± 0.2	1.25 ± 0.27
11.013	0.53 ± 0.11	3.5 ± 0.3	0.57 ± 0.13

TABLE 2
Excitation energies of the observed states in the high resolution ^{58}Ni(e, e′) reaction

E_x [MeV]	J^π	E_x [MeV]	J^π	E_x [MeV]	J^π
5.909	2^+	9.755	$1^+, (2^-)$	12.447	(2^+)
5.934	*	9.799	*	12.482	$(2^+, 4^+)$
5.967	$2^+, 3^-$	9.846	1^+	12.573	$2^+, 3^-$
6.031	$(1^-), 2^+$	9.870	(2^-)	12.613	2^+
6.182	$2^+, 3^-$	9.941	$(1^-), 2^+$	12.647	$2^+, (4^+)$
6.235	$(1^-), 2^+$	10.036	(2^-)	12.700	$(1^+), 2^-$
6.310	$1^-, 2^+$	10.073	1^+	12.746	(2^+)
6.417	2^+	10.105	1^+	12.796	$1^+, (2^-)$
6.475	$1^+, (2^-)$	10.157	1^+	12.837	(2^+)
6.729	$2^+, 3^-$	10.218	1^+	12.858	2^+
6.768	*	10.266	1^+	12.931	$2^+, 3^-$
6.816	$(1^-), 2^+$	10.355	1^+	12.971	2^+
6.851	3^-	10.385	$1^+, (2^-)$	13.022	$2^+, 4^+$
6.981	2^+	10.438	$(1^-), 2^+$	13.057	2^+
7.051	*	10.514	1^+	13.125	*
7.109	2^+	10.550	$(1^+, 2^-)$	13.176	$1^+, (2^-)$
7.209	3^-	10.582	$1^+, (2^-)$	13.233	2^+
7.255	2^+	10.633	1^+	13.260	2^+
7.290	*	10.670	1^+	13.305	(2^+)
7.388	1^+	10.720	$(3^-, 4^+)$	13.345	2^+
7.470	$1^+, (2^-)$	10.743	*	13.411	1^+
7.500	3^-	10.806	$1^+, 2^-$	13.448	2^+
7.560	1^+	10.856	$(1^-, 2^+)$	13.492	*
7.603	(1^-)	10.891	2^+	13.556	$(1^-), 2^+$
7.684	1^-	10.950	1^+	13.590	$(1^+, 2^-)$
7.715	1^+	11.013	1^+	13.649	2^+
7.746	$(1^+, 2^-)$	11.041	(2^+)	13.685	(2^+)
7.820	*	11.080	$1^+, (2^-)$	13.716	1^+
8.240	1^+	11.135	$(3^-, 4^+)$	13.765	$1^+, (2^-)$
8.276	$1^+, (2^-)$	11.160	$2^+, 3^-$	13.814	2^+
8.395	2^+	11.265	$1^+, (2^-)$	13.902	$2^+, (3^-)$
8.475	2^-	11.297	2^+	13.929	(2^+)
8.516	1^+	11.330	$1^-, 2^+$	13.955	(2^+)
8.601	1^+	11.363	$(1^+), 2^-$	14.000	2^+
8.680	1^+	11.410	$(2^+, 3^-)$	14.045	(2^+)
8.780	2^-	11.470	$(1^+), 2^-$	14.081	1^+
8.817	$1^+, (2^-)$	11.536	$(1^+), 2^-$	14.138	*
8.854	$2^+, 3^-$	11.597	2^+	14.180	$1^+, (2^-)$
8.875	1^+	11.639	$2^+, 3^-$	14.213	(2^+)
8.926	(1^-)	11.680	1^+	14.272	$1^-, 2^+, 3^-$
8.967	$1^+, (2^-)$	11.734	2^+	14.303	$1^-, 2^+, 3^-$
9.037	$1^+, (2^-)$	11.800	(2^+)	14.337	2^+
9.073	1^+	11.860	1^+	14.383	2^+
9.113	*	11.890	$(1^+), 2^-$	14.441	$2^+, (3^-)$
9.163	1^+	11.933	$(3^-, 4^+)$	14.504	2^+
9.260	*	11.990	$1^+, (2^-)$	14.542	$(1^-), 2^+, (3^-)$
9.298	*	12.040	2^+	14.598	*
9.368	$1^+, (2^-)$	12.090	*	14.630	$2^+, 3^-$
9.407	$(1^+), 2^-$	12.141	$1^-, 2^+$	14.692	*
9.468	*	12.197	(2^+)	14.736	(2^+)
9.513	$1^+, (2^-)$	12.249	*	14.823	2^+
9.552	(2^-)	12.280	(1^-)	14.852	$1^+, (2^-)$
9.643	$(1^+), 2^-$	12.330	$(1^+), 2^-$	14.894	$1^-, 2^+$
9.667	2^-	12.386	(2^+)	14.940	(2^+)

The J^π values have been determined through a comparison of the measured cross sections with DWBA (and sometimes also PWPA) calculations. An asterisk denotes the cases for which no assignment of J^π has been possible.

excitation energies. In addition, the survey spectrum displayed in fig. 3 shows transitions into states at $E_x = 2.775$ MeV (2^+), 3.040 MeV (2^+), 3.266 MeV (2^+), 3.533 MeV (0^+), 3.902 MeV (2^+) and 4.111 MeV $(2^+, 4^+)$. The comparison with values from the literature [25-30]) demonstrates an excellent agreement of 2-3 keV of the respective excitation energies and yields the J^π assignments given in parenthesis.

As can be seen from table 2, 47 levels were given the assignment $J^\pi = 1^+$. They are listed separately in table 3 together with their corresponding M1 strengths. The indicated uncertainties are due to stastistical errors only. The summed transition strengths of all states amounts to $\Sigma B(\mathrm{M1})\uparrow = 16.9^{+4.6}_{-3.3}\mu_N^2$. The strength of uncertain $J^\pi = 1^+$ candidates of levels (see table 2) has thereby been weighted by the factor 0.2 and been added linearly to the upper value of the error.

This M1 strength distribution is discussed in detail in the next section.

3. Discussion

3.1. M1 STRENGTH DISTRIBUTION

The distribution of magnetic dipole strength as listed in table 3 is shown in the upper part of fig. 8. It is the most structured M1 strength distribution known so far.

TABLE 3

Excitation energies and transition strengths of the detected M1 transitions in ^{58}Ni

E_x [MeV]	$B(\mathrm{M1})\uparrow$ [μ_N^2]	E_x [MeV]	$B(\mathrm{M1})\uparrow$ [μ_N^2]
6.475	0.17 ± 0.05	10.266	0.22 ± 0.04
7.388	0.33 ± 0.07	10.355	0.24 ± 0.03
7.470	0.25 ± 0.05	10.385	0.15 ± 0.03
7.560	0.15 ± 0.04	10.514	0.40 ± 0.03
7.715	0.74 ± 0.05	10.582	0.22 ± 0.03
8.240	1.27 ± 0.20	10.633	0.32 ± 0.12
8.276	0.26 ± 0.03	10.670	1.25 ± 0.06
8.516	1.04 ± 0.15	10.806	0.12 ± 0.04
8.601	0.44 ± 0.05	10.950	0.20 ± 0.04
8.680	0.47 ± 0.03	11.013	0.57 ± 0.03
8.817	0.19 ± 0.02	11.080	0.22 ± 0.07
8.875	0.51 ± 0.04	11.265	0.11 ± 0.02
8.967	0.23 ± 0.06	11.680	0.17 ± 0.03
9.037	0.30 ± 0.04	11.860	0.43 ± 0.29
9.073	0.26 ± 0.05	11.990	0.32 ± 0.06
9.163	0.23 ± 0.03	12.796	0.47 ± 0.09
9.368	0.34 ± 0.04	13.176	0.37 ± 0.06
9.513	0.22 ± 0.15	13.411	0.14 ± 0.03
9.755	0.32 ± 0.05	13.716	0.30 ± 0.02
9.846	0.54 ± 0.07	13.765	0.33 ± 0.06
10.073	0.35 ± 0.03	14.081	0.22 ± 0.05
10.105	0.21 ± 0.02	14.180	0.22 ± 0.02
10.157	0.37 ± 0.04	14.852	0.20 ± 0.04
10.218	0.56 ± 0.04		

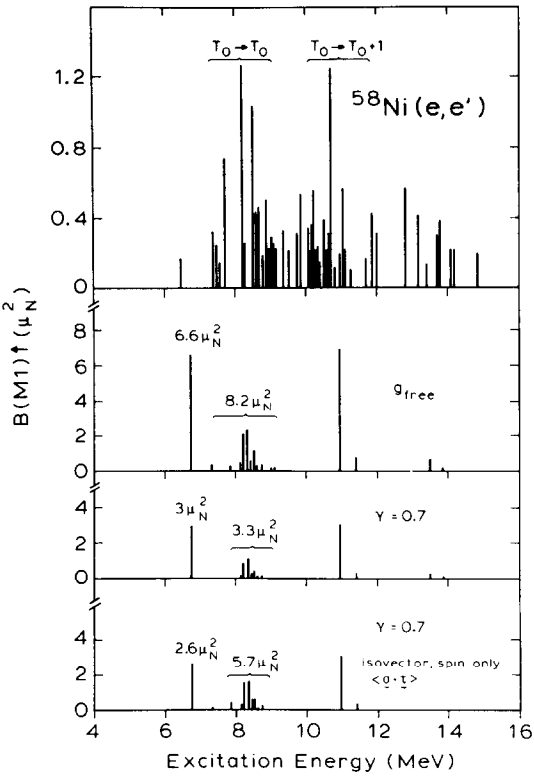

Fig. 8. Highly fragmented M1 strength distribution (upper part) as measured in ^{58}Ni(e, e') compared to a shell model calculation with the full electromagnetic M1 operator (g_{free}), a quenched operator ($\gamma = 0.7$) and with the quenched $\boldsymbol{\sigma} \cdot \boldsymbol{\tau}$ operator only (all in succession below the experimental strength distribution).

As a gross feature two humps at the center-of-gravity energies $E_x \approx 8.4$ and 11.4 MeV emerge. On the basis of results from ^{58}Ni(p, p') studies [10]) and from the ^{58}Ni(t, ^{3}He)^{58}Co reactions [16]) we identify these humps as the $T_0 \rightarrow T_0$ and $T_0 \rightarrow T_0+1$ isospin components of the M1 excitation. The overall center of gravity of the M1 strength is at $E_x \approx 10.2$ MeV in excellent agreement with the simple rule for $0\hbar\omega$ M1 transitions, i.e. $E_x \approx 40A^{-1/3}$ MeV.

The summed strength for the excitation of all $J^\pi = 1^+$ states $\sum B(\mathrm{M1})\uparrow = 16.9^{+4.6}_{-3.3}\mu_N^2$ exhausts between 57-90% of the shell model value to be discussed below. The corresponding quenching factor of the transition strength $\gamma = 0.8 \pm 0.1$ lies within the systematics of medium heavy nuclei [9]).

3.2. COMPARISON TO SHELL MODEL CALCULATIONS

The most simple interpretation of the two humps in the strength distribution of fig. 8 is offered by the one-particle, one-hole model, where they correspond to the

$[(2p_{3/2})^2_{0,1}(1f^{-1}_{7/2}1f_{5/2})_{1,1}]_{J^\pi,T=1^+,1}$ and $[(2p_{3/2})^2_{0,1},(1f^{-1}_{7/2}1f_{5/2})_{1,1}]_{J^\pi,T=1^+,2}$ configurations, respectively, that are the possible $1f^{-1}_{7/2}1f_{5/2}$ particle hole excitations of the $(2p_{3/2})^2_{0,1}$ ground state. In reality the observed fragmentation of the M1 strength can then be understood as the coupling of these doorway states to more complicated many particle, many hole configurations. Indeed, the spreading of strength is accounted for in a phenomenological doorway model (similar as for the very fragmented E2 giant resonance in ^{208}Pb [ref. [30]]) as has been shown elsewhere [31]).

In order to interpret the strength distribution in the upper part of fig. 8 more microscopically shell model calculations have been performed within a model space that includes all $(2p_{3/2}, 1f_{5/2}, 2p_{1/2})^2$ and $1f^{-1}_{7/2}(2p_{3/2}, 1f_{5/2}, 2p_{1/2})^3$ configurations. As a residual interaction the MSDI was used, for details see ref. [11]). The resulting strength distribution is shown below the experimental one in fig. 8. The pattern obtained is rather similar to that of the 1p-1h model, except for the transition strength between the two prominent peaks due to the $f_{7/2} \rightarrow f_{5/2}$ $\Delta T = 0$ and $\Delta T = 1$ spin-flip transitions. The total strength $\sum B(M1)\uparrow = 23.9\mu_N^2$ overestimates the experimental strength, as mentioned above.

We further investigated within this model the interference between spin and orbital magnetism. By renormalizing the spin part of the transition operator according to $g_s^{\text{eff}} = \gamma g_s^{\text{free}}$ with $\gamma = 0.7$, we obtain a state dependent renormalization of the transition strength. As is seen in fig. 8, the two strongest transitions at $E_x \approx 7$ and 11 MeV are reduced by a factor of two compared to a factor of about 3 for the group of weaker transitions around $E_x \approx 8.5$ MeV. If in addition the orbital part of the transition operator is switched off, the two strong transitions are unaffected whereas the transitions between them obtain almost the double strength. We therefore conclude that between the two doorway states a destructive interference between spin and orbital magnetism must be active. We return to this point below in connection with a comparison of the (e, e′) and (p, p′) results.

3.3. COMPARISON TO RESULTS FROM OTHER SPIN-FLIP PROBES

3.3.1. Inelastic proton scattering. High resolution inelastic proton scattering on ^{58}Ni has been performed at various incident energies. Measurements at $E_0 = 27$ MeV and $\Theta = 25°$ have identified two $J^\pi = 1^+$ states at $E_x = 2.903$ and 3.594 MeV [ref. [29])]. These states are also seen at $E_0 = 45$ MeV [ref. [32])]. An additional 1^+ state at the fairly low excitation energy of $E_x = 5.166$ MeV has been observed in a $E_0 = 65$ MeV measurement [33]). The isobaric analogue state of this state is known from the ^{58}Ni(p, n)^{58}Cu reaction [34]). Unfortunately, all these experiments at low bombarding energies are not very sensitive with respect to excitation of $J^\pi = 1^+$ states because of the nature of the effective nucleon-nucleus interaction [35]). However, at $E_0 \approx$ 200 MeV the $V_{\sigma\tau}$ term is dominant. This implies that at these energies and forward angle scattering $J^\pi = 1^+$ states are selectively excited. This can be seen in fig. 9 where a low energy backward angle (e, e′) spectrum is compared to a high energy forward

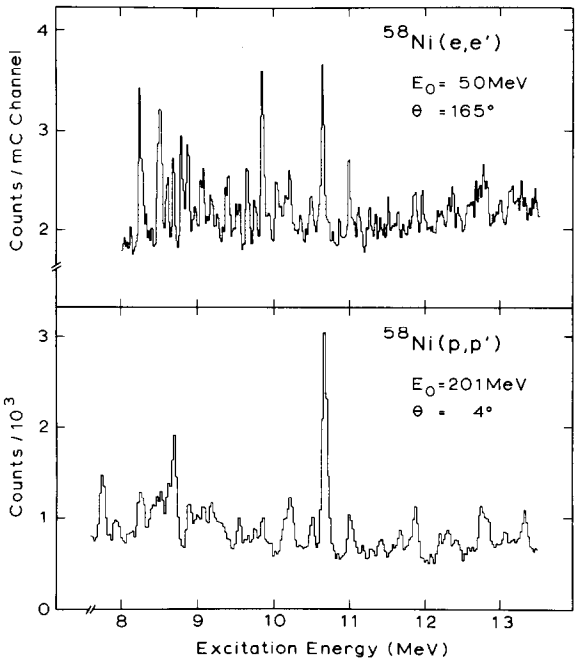

Fig. 9. Comparison of a backward angle high resolution (e, e') spectrum with a forward angle high resolution (p, p') spectrum (adapted from ref. [36]).

angle (p, p') spectrum [36]). Note the difference in energy resolution, i.e. $\Delta E_{1/2} \approx 30$ keV in (e, e') against ≈ 70 keV in (p, p'). A part of the difference in the structure of the spectra below $E_x \approx 10$ MeV is certainly due to the additional presence of $J^\pi = 2^-$ states in the (e, e') spectrum. Above this excitation energy the spectra are rather similar.

A more quantitative comparison of the results of the two experiments is made in fig. 10, where the M1 strength distribution from (e, e') is compared to the forward angle (p, p') cross sections. In the energy region up to $E_x = 9.5$ MeV both distributions were summed in 0.5 MeV bins (as done for (p, p') in ref. [10])) and normalized to the maximum. Above $E_x = 9.5$ MeV the normalization was performed at the strongest transition at $E_x = 10.67$ MeV. The following observations are made: (i) Due to the higher energy resolution more fine structure is obtained in (e, e'), however more recent but still preliminary results [37]) indicate that almost all 1^+ states seen in (e, e') are also observed in (p, p') at roughly the same excitation energy, the latter reaction showing even more 1^+ states than the former above $E_x \approx 12$ MeV. (ii) The gross structure of the two distributions is rather similar. (iii) The differences especially between $E_x \approx 8$–10 MeV can be attributed to the destructive interference between spin and orbital magnetization in (e, e') as pointed out above. A more detailed investigation would require a comparable energy resolution of (p, p') and (e, e') as

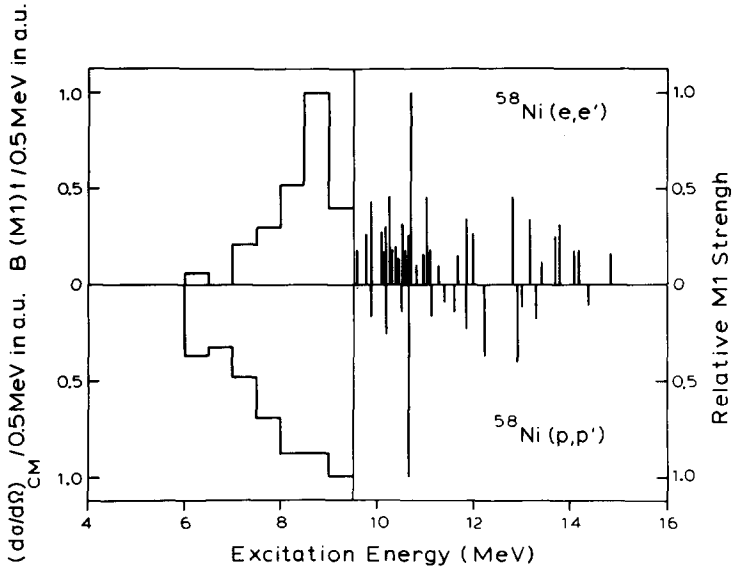

Fig. 10. Comparison of the M1 strength distribution determined from the present ^{58}Ni(e, e') experiment (upper part) with forward angle differential cross sections [10]) of $\Delta L = 0$ transitions (lower part). Up to $E_x = 9.5$ MeV all $B(M1)\uparrow$ values have been summed up in 0.5 MeV bins as were the cross sections in ref. [10]). The two quantities were normalized at the maximum ($E_x = 8.5$–9.0 MeV). For the region $E_x >$ 9.5 MeV both distributions have been normalized to each other utilizing the strogest transition $E_x =$ 10.670 MeV.

well as an improved microscopic description of the strength distribution within the shell model. In passing, we like to point out that similar intereference effects have been found in the M1 strength distributions on ^{52}Cr and ^{54}Fe [ref. [7])].

3.3.2. Charge exchange reactions. The J^π; $T = 1^+$; 2 states in ^{58}Ni have isobaric analogue states in ^{58}Co, which have been studied in the charge exchange reactions ^{58}Ni(t, ^{3}He) [refs. [16,38])], ^{58}Fe(p, n) [ref. [39])] and ^{58}Fe(^{3}He, t) [ref. [40])]. These $T = 2$ states are also seen (amongst $T = 0$ and $T = 1$ states) in the ^{58}Ni(p, n) reaction. Both experiments performed at high bombarding energies [34,36,41]), however, suffer from insufficient energy resolution to already allow a quantitative comparison with the present high resolution (e, e') results.

We have used the $J^\pi = 1^+$ assignment in the ^{58}Ni(t, ^{3}He) reaction [16]) to identify the J^π; $T = 1^+$; 2 analogue states in ^{58}Ni (see table 4). From the mean energy shift of $\Delta\bar{E}_x = 8.785 \pm 0.010$ MeV one obtains a Coulomb energy difference between ^{58}Ni and ^{58}Co of $\Delta E_c = 9.187 \pm 0.010$ MeV. The summed M1 strength carried by these $T = 2$ states is $\Sigma B(M1)\uparrow_{T=2} \approx 3.7\mu_N^2$. This implies that the ratio

$$R = \sum B(M1)\uparrow_{T=2} / \sum B(M1)\uparrow_{T=1} \approx 0.28$$

is in good agreement with the corresponding cross section ratio [10]) in (p, p') as well

TABLE 4

Excitation energies and relative cross sections of $J^\pi = 1^+$ states in ^{58}Co (first two columns) from the ^{58}Ni(t, ^{3}He)^{58}Co reaction [16]) and excitation energies, J^π values and M1 strengths in ^{58}Ni from the present ^{58}Ni(e, e') reaction (next three columns). The last column contains the excitation energy differences between the isobaric analogue 1^+ states.

E_x [MeV]	σ_{rel}	E_x [MeV]	J^π	$B(M1)\uparrow[\mu_N^2]$	ΔE_x [MeV]
1.050	1.08 ± 0.22	9.846	1^+	0.54 ± 0.07	8.796
1.377	0.16 ± 0.22	10.157	1^+	0.37 ± 0.04	8.780
1.436	0.23 ± 0.20	10.218	1^+	0.56 ± 0.05	8.781
1.729	1.06 ± 0.19	10.514	1^+	0.40 ± 0.03	8.785
1.865	1.93 ± 0.23	10.670	1^+	1.25 ± 0.06	8.805
2.249	0.25 ± 0.05	11.013	1^+	0.57 ± 0.03	8.764

as the results from the present shell model calculation, but this ratio disagrees with predictions from refs. [42,43]). However, if one assumes that all 1^+ states above $E_x \approx 9.5$ MeV in ^{58}Ni possess isospin $T = 2$ (the weakly excited states in (e, e') could e.g. have large orbital components and would not be observable in the charge exchange reactions) then we obtain a ratio $R \approx 1$ which would agree with the result of refs. [42,43]). We are therefore confronted with a puzzle which has further consequences for the isospin splitting of $T = T_0$ and $T = T_0 + 1$ states in ^{58}Ni. Assuming again that all states above $E_x = 9.5$ MeV have isospin $T = 2$ we obtain the center of gravities $\bar{E}_x(T_0) = 8.4$ MeV and $\bar{E}_x(T_0 + 1) = 11.4$ MeV in agreement with the values from

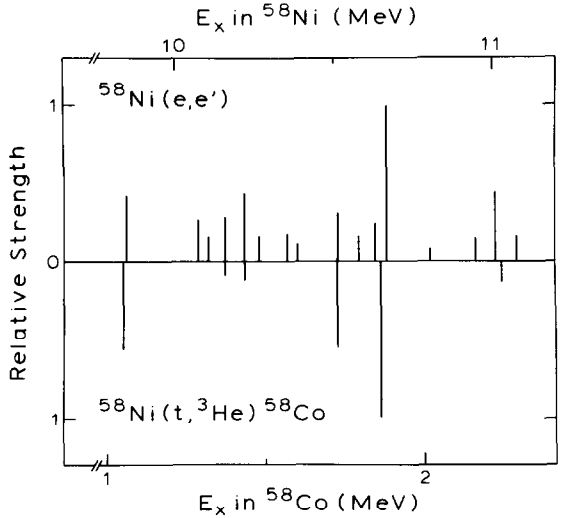

Fig. 11. Comparison of the relative strengths of $J^\pi = 1^+$ isobaric analogue States excited in the ^{58}Ni(e, e') and ^{58}Ni(t, ^{3}He)^{58}Co reaction, respectively. The distributions are normalized to each other at the strongest excited state.

inelastic proton scattering [44]). This leads to a depth of the Lane potential $V_1 = 87$ MeV in accordance with the estimates from ref. [45]).

We finally comment briefly on the importance of the present M1 strengths in the connection with the problem of an absolute calibration of Gamow-Teller transition strength relevant for astrophysical purposes. For the dynamics in supernovae a crucial ingredient is the absolute rate for the electron capture process ${}_ZA_N(e^-, \nu_e)_{Z-1}A_{N+1}$ (see refs. [12-19])). The Gamow-Teller part of the electron capture transition operator can be probed by a reaction like ${}_ZA_N(t, {}^3He)_{Z-1}A_{N+1}$. This has been done in ref. [16]), however, without an absolute calibration. Such a calibration is provided to some extent by relating the charge exchange cross sections to the measured M1 transition strength. Table 4 summarizes the results of the population of 1^+ states in a ^{58}Ni(t, ^{3}He)^{58}Co experiment in comparison with the excitation energies and M1 strengths of the present ^{58}Ni(e, e') experiment. The way the relative cross sections in the (t, ^{3}He) reaction behave as compared to the analogous (e, e') transition strength is noticeable and is illustrated again in fig. 11. There the two distributions normalized to the strongest excited state in ^{58}Co and ^{58}Ni are shown as mirror images. In addition to the 1^+ states listed in table 4 all other 1^+ states seen in (e, e') in this excitation energy region are also shown. One should of course remember the above discussion concerning the orbital contributions to the (e, e') strength which are absent in the (t, ^{3}He) reaction, but the pattern of the observed analogous transitions in the two reactions is quite similar.

4. Conclusion

The fragmentation of magnetic dipole strength in ^{58}Ni has been studied at low momentum transfer with high resolution inelastic electron scattering. The richness of fine structure in the resulting strength distribution is remarkable and has hitherto not been observed in any other nucleus. Large-space shell model calculations account for the general pattern of the detected M1 giant resonance in ^{58}Ni but a quenching of the observed transition strength compared to its predicted value is evident as in various other previously investigated fp-shell nuclei. A detailed comparison between the present (e, e') results with results from hadron scattering and charge exchange reactions has furthermore given valuable information on the isospin structure of the M1 giant resonance in ^{58}Ni. It is hoped that improved nuclear structure calculations as well as better inelastic electron scattering experiments - coincidence experiments of the (e, e'x) type on c.w. electron accelerators - probing the nuclear continuum in the future will be able to solve in particular the problem of missing strength.

We thank E.R. Flynn, P. Manakos, H. Spangenberger and W. Steffen for helpful discussions, N. Marty for letting us have preliminary results on the ^{58}Ni(p, p') experiment and D. Langheim for her efficient typing of the manuscript. We are also

very grateful to E. Spamer and the DALINAC crew for their continuous effort in the very long runs.

References

1) W. Gross, D. Meuer, A. Richter, E. Spamer, O. Titze and W. Knüpfer, Phys. Lett. **84B** (1979) 296
2) W. Steffen, H.-D. Gräf, W. Gross, D. Meuer, A. Richter, E. Spamer, O. Titze and W. Knüpfer, Phys. Lett. **95B** (1980) 23
3) W. Steffen, R. Benz, S. Müller, A. Richter and W. Knüpfer, to be published
4) W. Steffen, H.-D. Gräf, A. Richter, A. Härting, W. Weise, U. Deutschmann, G. Lahm and R. Neuhausen, Nucl. Phys. **A404** (1983) 413
5) G. Eulenberg, D.I. Sober, W. Steffen, H.-D. Gräf, G. Küchler, A. Richter, E. Spamer, B.C. Metsch and W. Knüpfer, Phys. Lett. **116B** (1982) 113
6) D. Bender, G. Eulenberg, A. Richter, E. Spamer, B.C. Metsch and W. Knüpfer, Nucl. Phys. **A398** (1983) 408
7) D.I. Sober, B.C. Metsch, W. Knüpfer, G. Eulenberg, G. Küchler, A. Richter, E. Spamer and W. Steffen, Phys. Rev. **C31** (1985) 2054
8) R.A. Lindgren, W.L. Bendel, E.C. Jones, Jr., L.W. Fagg, X.K. Maruyama, J.W. Lightbody, Jr. and S.P. Fivozinsky, Phys. Rev. **C14** (1976) 1789
9) A. Richter, Phys. Scripta **T5** (1983) 63
10) N. Marty, C. Djalali, M. Morlet, A. Willis, J.C. Jourdain, N. Anantaraman, G.M. Crawley, A. Galonsky, Nucl. Phys. **A396** (1983) 145c
11) A.G.M. van Hees, P.W.M. Glaudemans and B.C. Metsch, Z. Phys. **A293** (1979) 327
12) H.A. Bethe, G.E. Brown, J. Applegate and J.M. Lattimer, Nucl. Phys. **1324** (1979) 487
13) G.M. Fuller, W.A. Fowler and M.J. Newman, Astrophys. J. **252** (1982) 715
14) G.M. Fuller, W.A. Fowler and M.J. Newman, Astrophys. J. Suppl. **42** (1980) 447
15) F. Ajzenberg-Selove and E.K. Warburton, Phys. Today, November (1983) 26
16) F. Ajzenberg-Selove, R.E. Brown, E.R. Flynn and J.W. Sunier, Phys. Rev. **C30** (1984) 1850; Phys. Rev. **C31** (1985) 777
17) A. Zaringhalam, Nucl. Phys. **A404** (1983) 599
18) J. Cooperstein and J. Wambach, Nucl. Phys. **A420** (1984) 591
19) S.D. Bloom and G.M. Fuller, Nucl. Phys. **A440** (1985) 511
20) H.-D. Gräf, H. Miska, E. Spamer, O. Titze and Th. Walcher, Nucl. Instr. Meth. **153** (1978) 9;
Th. Walcher, R. Frey, H.-D. Gräf, E. Spamer and H. Theissen, Nucl. Instr. Meth. **153** (1978) 17;
D. Schüll, J. Foh, H.-D. Gräf, H. Miska, R. Schneider, E. Spamer, H. Theissen, O. Titze and Th. Walcher, Nucl. Instr. Meth. **153** (1978) 29;
J. Foh, R. Frey, R. Schneider, D. Schüll, A. Schwierczinski, H. Theissen and O. Titze, Nucl. Instr. Meth. **153** (1978) 43
21) D. Meuer, R. Frey, D.H.H. Hoffmann, A. Richter, E. Spamer, O. Titze and W. Knüpfer, Nucl. Phys. **A349** (1980) 309
22) C.W. de Jager, H. de Vries and C. de Vries, Atomic Data and Nucl. Data Tables **14** (1974) 479
23) S.T. Tuan, L.E. Wright and D.S. Onley, Nucl. Instr. Meth. **60** (1968) 70
24) H. Theissen, Springer Tracts in Modern Physics **65** (1972) 1
25) G. Bruge, A. Chaumeaux, R. de Vries and G.C. Morrison, Phys. Rev. Lett. **29** (1972) 295
26) D.H. Kong-A-Sion, A.J. Cole, A. Giorni and J.P. Longequeve, Nucl. Phys. **A221** (1974) 45
27) D.C. Kocher and R.C. Auble, Nucl. Data Sheets **19** (1976) 445
28) G.S. Kyle, N.M. Hintz, M.S. Outhoudt, M. Kaletka, P.M. Lang, H. Nann, K.K. Seth, D.K. McDaniels, P.M. Varghese, T. Kozlowski, D.G. Madland, C.L. Morris, J.C. Pratt, J.E. Spencer, N. Tanaka, H.A. Thiessen, G.S. Blanpied, G.W. Hoffmann, R.P. Liljestrand, J.C. Fong, G. Igo, R.J. Ridge and C. Whitten Jr., Phys. Lett. **91B** (1980) 353
29) H.P. Blok, J.J. Kraushaar, P.A. Batay-Csorba and F.E. Cecil, Nucl. Phys. **A386** (1982) 61
30) J. Winchenbach, K. Pingel, G. Holzwarth, G. Kühner and A. Richter, Nucl. Phys. **A410** (1983) 237
31) H. Spangenberger, F. Beck and A. Richter, Nucl. Phys. **A448** (1986) 21

32) G.P.A. Berg, G. Gaul, J. Meissburger, D. Paul, J.G.M. Römer, G. Sondermann and J.L. Tain. KFA Institut für Kernphysik, Annual Report (1983) p. 2
33) M. Fujiwara, Y. Fujita, I. Katayama, S. Morinobu, T. Yamazaki, H. Ikegami, S.I. Hayakawa and K. Katori, Nucl. Phys. **A410** (1983) 139
34) J. Rapaport, T. Taddeucci, T.P. Welch, D.J. Horen, J.B. McGrory, C. Gaarde, J. Larsen, E. Sugarbaker, P. Koncz, C.C. Foster, C.D. Goodman, C.A. Goulding and T. Masterson, Phys. Lett. **119B** (1982) 61
35) W.G. Love and M.A. Franey, Phys. Rev. **C24** (1981) 1073
36) N. Anantaraman, G.M. Crawley, A. Galonsky, C. Djalali, N. Marty, A. Willis, J.C. Jourdain and P. Kitching, Annual Report of the Michigan State University, East Lansing, Michigan, USA (1981)
37) N. Marty, private communication
38) E.R. Flynn and J.D. Garrett, Phys. Rev. Lett. **29** (1972) 1748
39) A. Park, E. Sugarbaker, R.A. Emigh, C.A. Fields and P.A. Smith, University of Colorado, Nuclear Physics Laboratory technical progress report (1979), C00-535-767
40) C. Wong, S.D. Bloom, S.M. Grimes, R.F. Hausmann, Jr. and V.A. Madsen, Phys. Rev. **C18** (1978) 2052
41) J.R. Rapaport, T. Taddeucci, T.P. Welch, C. Gaarde, J. Larsen, D.J. Horen, E. Sugarbaker, P. Kuncz, C.C. Forster, C.D. Goodman, C.A. Goulding and T. Masterson, Nucl. Phys. **A410** (1983) 371
42) S. Fallieros and B. Goulard, Nucl. Phys. **A147** (1970) 593
43) E. Lipparini, S. Stringari, M. Traini and R. Leonardi, Nuov. Cim. **31A** (1976) 207
44) C. Djalali, N. Marty, M. Morlet, A. Willis, J.C. Jourdain, N. Anantaraman, G.M. Crawley, A. Galonsky and P. Kitching, Nucl. Phys. **A388** (1982) 1
45) W.A. Sterrenburg, S.M. Austin, R.P. De Vito and A. Galonsky, Phys. Rev. Lett. **45** (1980) 1839